*Article*

# Abnormal Intrinsic Functional Hubs in Corneal Ulcer: Evidence from a Voxel-Wise Degree Centrality Analysis

**Min-Jie Chen** [†], **Rong Huang** [†], **Rong-Bin Liang** [†], **Yi-Cong Pan, Hui-Ye Shu, Xu-Lin Liao** [ID], **San-Hua Xu, Ping Ying, Min Kang, Li-Juan Zhang, Qian-Min Ge** [ID] **and Yi Shao** *,[‡] [ID]

Department of Ophthalmology, The First Affiliated Hospital of Nanchang University, Jiangxi Center of National Ocular Disease Clinical Research Center, Nanchang 330006, China; 1476053262@qq.com (M.-J.C.); huangrong807@163.com (R.H.); burbo986@163.com (R.-B.L.); pyccell2009@163.com (Y.-C.P.); iamshy0626@163.com (H.-Y.S.); liaoxulin@link.cuhk.edu.cn (X.-L.L.); xusanhua6196@163.com (S.-H.X.); yypp4562021@163.com (P.Y.); km991342@163.com (M.K.); zhanglj0551@163.com (L.-J.Z.); 411438819008@email.ncu.edu.cn (Q.-M.G.)
* Correspondence: freebee99@163.com
† These authors have contributed equally to this work.
‡ Current address: Department of Ophthalmology, The First Affiliated Hospital of Nanchang University, Jiangxi Province Clinical Ophthalmology Institute, 17 Yongwaizheng Street, Donghu, Nanchang 330006, China.

**Abstract:** Background: Numerous anterior neuroimaging researches have revealed that corneal ulcers (CU) are related to changes in cerebral anatomic structure and functional area. Nonetheless, functional characteristics of the brain's network organization still show no definite research results. The study was designed to confirm CU-associated spatial centrality distribution functional network of the whole cerebrum and explore the mechanism through which the larvaceous changed the intrinsic functional hubs. Material and Methods: In this study, 40 patients with CU and 40 normal controls (matched in sex, age, and education level) were enrolled in this study to undergo resting-state functional magnetic resonance imaging (fMRI) scans. The differences between the groups were determined by measuring the voxel-wise degree centrality (DC) throughout the whole cerebrum. For the purpose of assessing the correlation between abnormal DC value and clinical variables, the Linear correlation analysis was used. Results: Compared with normal controls (NCs), CU patients revealed high DC values in the frontal lobe, precuneus, inferior parietal lobule, posterior cingulate, occipital lobe, and temporal lobe in the brain functional connectivity maps throughout the brain. The intergroup differences also had high similarity on account of different thresholds. In addition, DC values were positively related to the duration of CU in the left middle frontal gyrus. Conclusions: The experimental results revealed that patients with CU showed spatially unnatural intrinsic functional hubs whether DC values increased or decreased. This brings us to a new level of comprehending the functional features of CU and may offer useful information to make us obtain a clear understanding of the dysfunction of CU.

**Keywords:** corneal ulcer; resting state; abnormal intrinsic functional hubs; degree centrality; voxel-wise

## 1. Introduction

Corneal ulcer (CU), including infectious and noninfectious CU, is a common ophthalmological disease worldwide, especially in developing countries, and is the main reason of corneal opacities as well as the fourth commonest reason of monocular blindness [1]. Common causes of corneal ulcer include microbial infection, which often leads to corneal purulence [2]. (Figure 1) Bacterial keratitis, if not treated promptly, can lead to endophthalmitis or even complete loss of vision [3]. Corneal scarring may also occur after treatment for corneal ulcers. Slit lamp and fluorescein staining are common methods for the diagnosis of CU [4,5], while genomic technology is also gradually applied for corneal ulcer and other ophthalmic diseases [6–8]. However, both methods focus on the anterior segment and

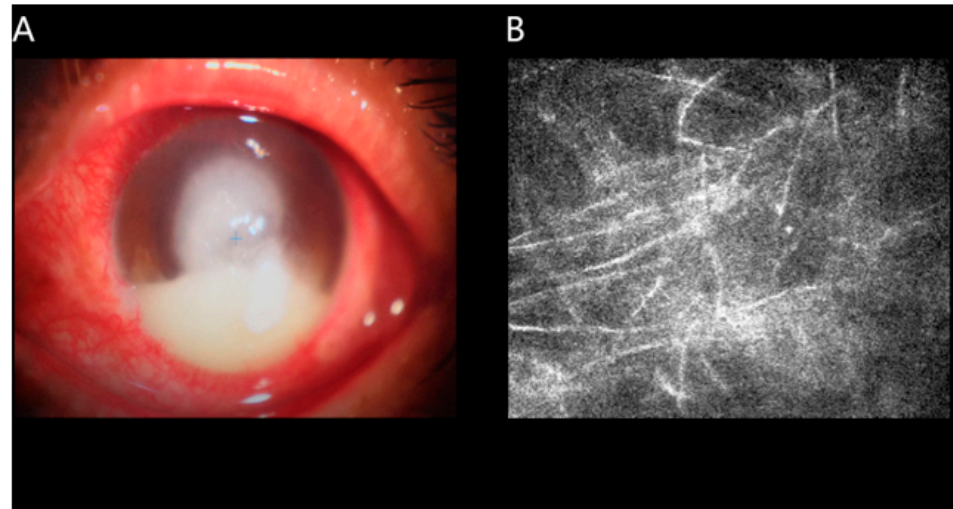overlook other areas also involved in visual system, especially ignoring the optic tract and visual cortex.



**Figure 1.** An example of UC detected with the use of slit lamp examination. Corneal infiltration was observed under the slit lamp. (**A,B**) shows confocal corneal microscopy of fungal keratitis.

Furthermore, the resting-state functional magnetic resonance imaging (fMRI) is a non-invasive neuroimaging mechanism that is always used to further infer the state of neural activity in specific cerebral areas by analyzing the level of blood oxygen metabolism. fMRI can detect the abnormality of cerebrum and enhances our understanding of ophthalmological diseases. There is considerable neuroimaging evidence from fMRI studies showing that ophthalmic patients may have neural tissue injury or cortical dysfunction [9].

Voxel-wise degree centrality (DC) can demonstrate our network structure at the voxel level of functional connection in the cerebrum of human beings. DC provides data regarding functional connectivity within the human cerebrum network instead of low-frequency fluctuation in regional homogeneity and amplitude [10]. Thus far, DC method has often been used for the investigation of the neuropathologic mechanisms of numerous diseases, including Parkinson's disease, obesity, and autism [11–13]. Similarly, the DC method has been used to study many eye diseases so far, such as in [14].

In our research, we examined the centrality spatial distribution of the functional network throughput the whole brain in patients with CU and tried to determine the relativity between intrinsic functional hubs and clinical characteristics and which was aimed to more accurately diagnose the disease severity of patients with corneal ulcer, delay the disease progression, and guide clinical treatment more effectively.

## 2. Material and Methods

### 2.1. Participants

Our study confirmed to the ethical standards of Declaration of Helsinki as well as ethical standards of medical ethics. Relevant research methods were performed under the permission of the committee of the medical ethics of our hospital (hidden for peer review) in our research. Participants enrolled in this research are voluntary and provided written informed consent.

In this research, totally 40 CU patients (26 males, 14 females) were included. Relevant inclusion criteria of the CU group were (1) significant degeneration and necrosis in the cornea detected through slit lamp examination (Figure 1) and (2) absence of other bilateral ocular diseases (e.g., cataracts, glaucoma, etc.).

The exclusion criteria were (1) high tendency of perforation, corneal perforating, and blindness; (2) ocular injury; (3) history of systemic diseases, just like cardiopathy; (4) psychosis; and (5) other factors that interfere with DC measurement.

Forty normal controls (NCs) (26 males, 14 females) were recruited in the study. In addition, in terms of sex, age, and level of education, they are precisely matched with the CU patients. NCs reached the following standards: (1) without neurological disease or psychosis (e.g., Parkinson's disease, depression, bipolar affective disorder, etc.) and (2) can be scanned with MRI (e.g., no metal products in the body, such as pacemakers, etc.).

### 2.2. MRI Parameters

We performed the MRI scanning by applying a 3-Tesla MR scanner (Trio, Siemens, Munich, Germany).The T1-weighted images of the whole brain were collected through a spoiled gradient-recalled echo sequence with appropriate parameters (i.e., repetition time: 1900 ms; echo time: 2.26 ms; thickness: 1.0 mm; gap: 0.5 mm; acquisition matrix: $256 \times 256$; field of view: $250 \times 250$ mm; flip angle: 9°). Functional images were collected with appropriate parameters (i.e., repetition time: 2000 ms; echo time: 30 ms; thickness: 4.0 mm; gap: 1.2 mm; acquisition matrix: $64 \times 64$; flip angle: 90°; field of view: $220 \times 220$ mm; 29 axial).

### 2.3. fMRI Data Processing

All data were pre-filtered with MRIcro (www.MRIcro.com, accessed on 5 January 2022) and pretreated through Statistical Parametric Mapping (SPM8, http://www.fil.ion.ucl.ac.uk/spm, accessed on 5 January 2022), Data Processing Assistant for Resting-State fMRI (DPARSFA, http://rfmri.org/DPARSF, accessed on 5 January 2022), and the Resting-state Data Analysis Toolkit (REST, http://www.restfmri.net, accessed on 5 January 2022). Deleting the first 10 time points, we then obtained the residual 230 volumes. Volumes with x, y, or z directions >2 were not taken into account. In a previous study [15], a detailed description of this method was provided.

### 2.4. DC

On the basis of the individual voxel-wise functional network, our research try to calculate DC through calculating the amount of meaningful suprathreshold correlations (or the degree of the binarized adjacency matrix) between participants. In our research, all the voxel-wise DC maps were transferred into z-score maps with the application of the following equation: $Z_i = DC_i$ meanall/stdall ($Z_i$ = the z score of its voxel; $DC_i$ = the DC value of its voxel; meanall = the mean DC value of all voxels in the brain mask; stdall = the standard deviation of the DC values of all voxels in the brain mask).

### 2.5. Statistical Analysis

In order to carry out demographic and clinical measurements, the SPSS version 19.0 software (IBM, Armonk, NY, USA) was utilized in the purpose of differentiating clinical features between the CU and NCs by performing, unaided, two-sample *t*-tests.

The spatial centrality distribution (hubs) throughout human cerebrum functional network was identified through one sample *t*-test for voxel-wise DC. Furthermore, two-sample *t*-tests were independently conducted, considering age, sex, and education level as interference variable in this research within the default gray matter mask. The main purpose of this operation was to assess the differences between groups in the voxel-wise DC through the application of the REST V1.8. ($p < 0.05$ for multiple comparisons with the use of Gaussian Random Field theory, z > 2.3, and cluster-wise corrected $p < 0.05$ denoted statistical significance).

Correlation analysis was applied for the purpose of evaluating the relativity of the average DC values and behavioral characteristics.

## 3. Results

### 3.1. Demographic Information and Visual Measurements

Between the two groups ($p > 0.05$), we can see from the Table 1 that there were no apparent differences either in weight ($p = 0.824$) or age ($p = 0.892$). Additionally, the average standard deviation of the duration of CU was $8.10 \pm 3.57$ days (Table 1).

**Table 1.** The conditions of participants included in the study.

| Condition | CUs | NCs | T | *p*-Value * |
|---|---|---|---|---|
| Male/female | 26/14 | 26/14 | N/A | >0.99 |
| Age (years) | $51.25 \pm 5.46$ | $51.98 \pm 5.18$ | 0.251 | 0.824 |
| Weight (kg) | $63.12 \pm 7.35$ | $63.89 \pm 6.73$ | 0.181 | 0.892 |
| Handedness | 40R | 40R | N/A | >0.99 |
| Duration of CU (days) | $8.10 \pm 3.57$ | N/A | N/A | N/A |

* $p < 0.05$, independent *t*-tests comparing two groups. Abbreviations: NC, normal controls; N/A, not applicable; CU, corneal ulcer.

### 3.2. Differences in DC

The distributions of the functional centers (high degree centrality) of CU patients were highly similar with NCs in spatial distribution and mainly located in the frontal lobe, precuneus, inferior parietal lobule, posterior cingulate, occipital lobe, and temporal lobe (Figures 2 and 3 (red) and Table 2). Intergroup differences, on the basis of the different correlation thresholds ($r_0 = 0.15, 0.2, 0.25, 0.3$, and $0.35$), were also largely similar (Figure 4). Hence, we mostly reported the value of DC when the correlation thresholds were set at the standards of 0.25 in the weighted graph. In DC of two groups, Figure 5A shows the average changes.

**Table 2.** Significant differences in DC between groups ($r_0 = 0.25$).

| Condition | L/R | Brain Regions | MNI Coordinates | | | Cluster Size | *t*-Value |
|---|---|---|---|---|---|---|---|
| | | | X | Y | Z | | |
| CU > NC | L | Cerebellum Posterior Lobe | −9 | −84 | −24 | 49 | 3.604 |
| CU > NC | R | Inferior Parietal Lobule | 48 | −63 | 42 | 72 | 3.526 |
| CU > NC | L | Middle Frontal Gyrus | −36 | 36 | 45 | 104 | 4.239 |
| CU > NC | L | Precuneus | −33 | −75 | 42 | 93 | 4.746 |
| CU > NC | L | superior parietal lobule | −3 | −75 | 48 | 61 | 4.975 |

Notes: $p < 0.01$, Cluster > 40 voxels, AlphaSim corrected. Abbreviations: NC, normal control; CU, corneal ulcer; MNI, Montreal Neurological Institute; L, left; R, right.

### 3.3. Correlation Analysis

We can see a positive correlation between DC values and the duration of CU in the left middle frontal gyrus ($r = 0.849$, $p < 0.001$) in the DC group (Figure 5B).

### 3.4. Receiver Operating Characteristic (ROC) Curve

It is speculated that DC can be used as significant biomarker in order to distinguish the CU group from the NC group. In different cerebrum areas, we utilized ROC curve in the purpose of evaluating the average DC values. The area under the ROC curve (AUC) indicated a diagnostic efficiency. AUC values 0.5–0.7, 0.7–0.9, and >0.9 indicated low, medium, and high accuracy, separately. The AUC values of DC in specific areas were showed as follows: left cerebellum posterior lobe (0.822), right inferior parietal lobule (0.788), left middle frontal gyrus (0.878), left precuneus (0.840), and left parietal lobe (0.842) (Figure 5C).
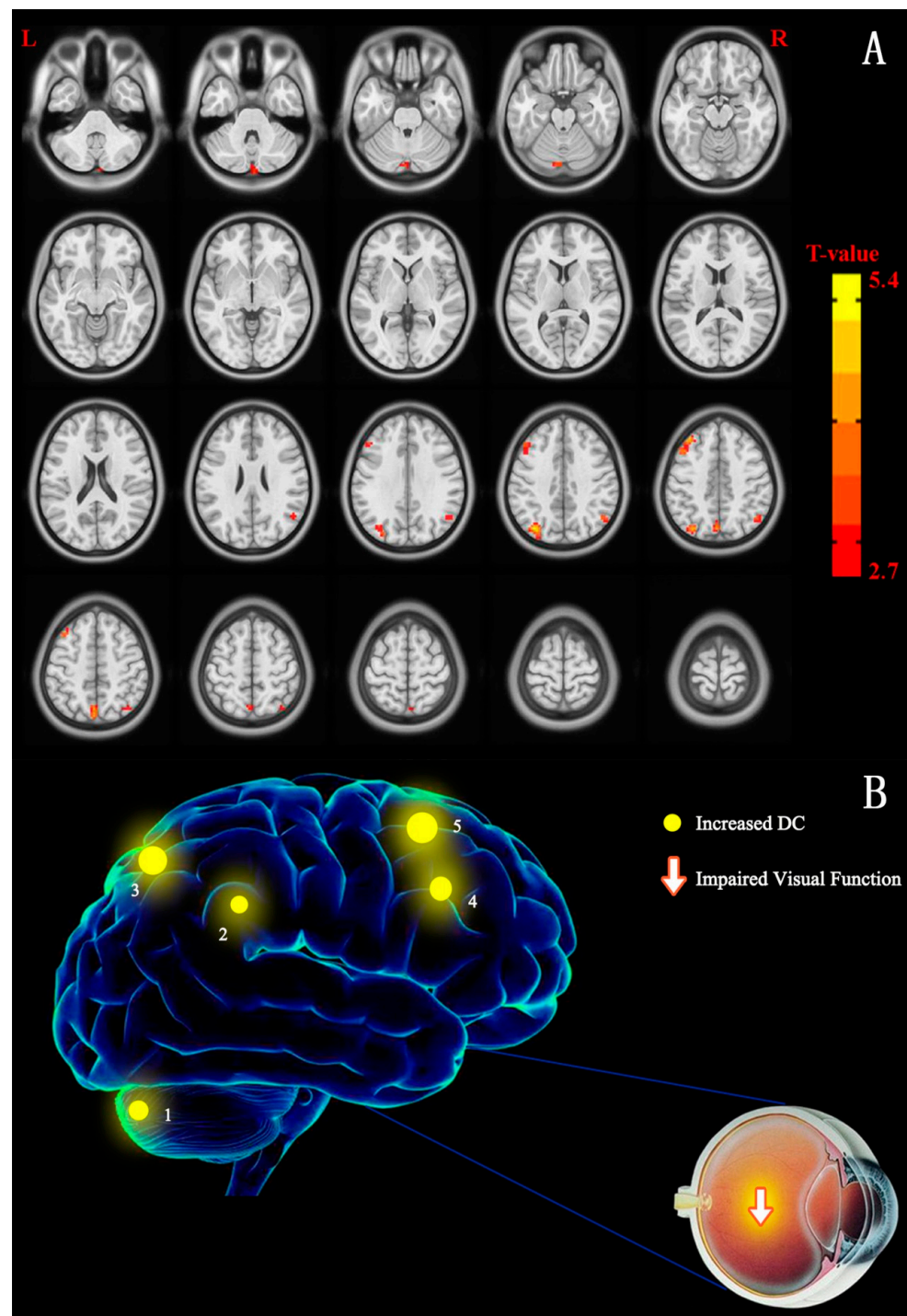
**Figure 2.** (**A**) Cross-section view: voxel-wise comparison of DC in CU and NC groups. DC values that have significant differences were observed in the frontal lobe, precuneus, inferior parietal lobule, posterior cingulate, occipital lobe, and temporal lobe. In the picture, the red and blue indicate increased and decreased DC values, respectively. Only increased DC values were recorded ($p < 0.01$, cluster > 40 voxels, AlphaSim corrected). (**B**) The DC values of cerebrum activity in CU group. In comparison with NCs, the DC values that have significant differences in these cerebrum areas were decreased to different degree in patients with CU: 1-cerebellum posterior lobe ($t = 3.604$), 2-superior parietal lobule ($t = 4.975$), 3-inferior parietal lobule ($t = 3.526$), 4-precuneus ($t = 4.746$), and 5-middle frontal gyrus ($t = 4.239$). Notes: The size of spots is used in the study to reflected the extents of quantitative changes. Abbreviations: CU, corneal ulcer; NCs, normal controls; DC, degree centrality.
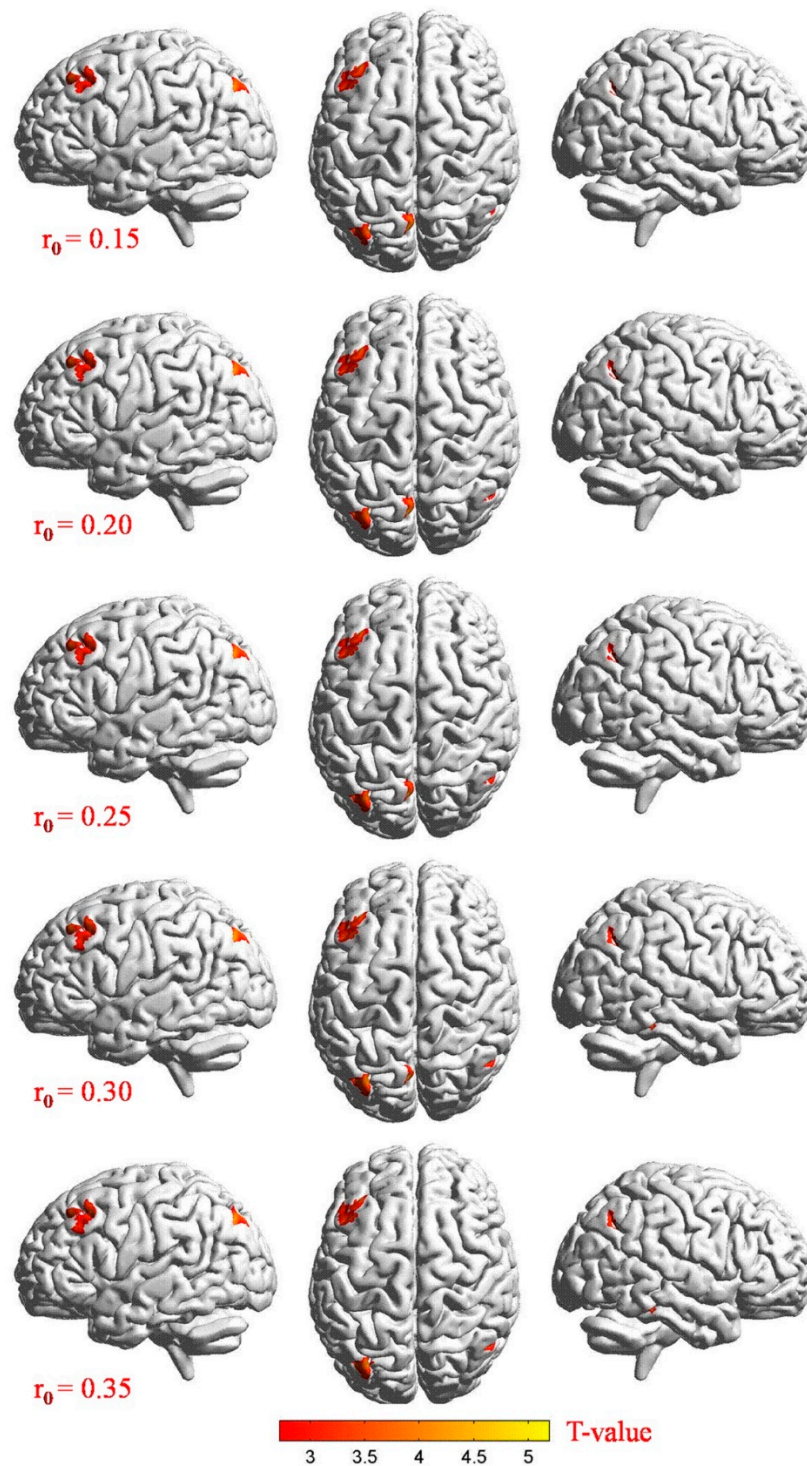
**Figure 3.** Stereoscopic view: voxel-wise comparison of DC values in two groups on the basis of different correlation thresholds ($r_0$ = 0.15, 0.2, 0.25, 0.3, and 0.35). In the frontal lobe, precuneus, inferior parietal lobule, posterior cingulate, occipital lobe, and temporal lobe, we detected significant differences in DC values. Increased and decreased DC values were clearly indicated through red and blue, respectively ($p < 0.01$, cluster > 40 voxels, AlphaSim corrected). Abbreviations: CU, corneal ulcer; NCs, normal controls; DC, degree centrality.
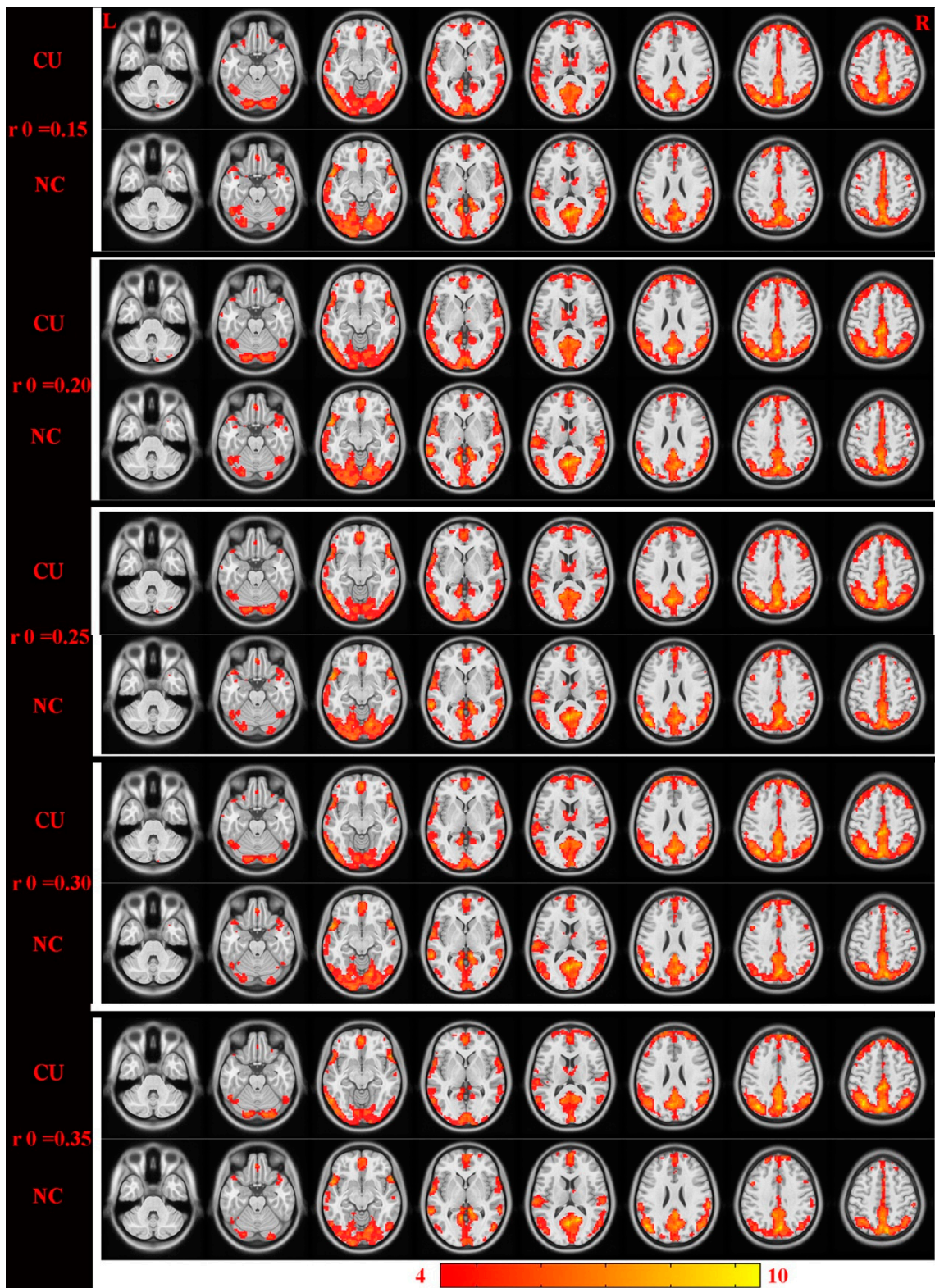
**Figure 4.** Cross-section view: intergroup differences were highly similar on the basis of different correlation thresholds ($r_0$ = 0.15, 0.2, 0.25, 0.3, and 0.35). DC values that have significant differences were detected in the frontal lobe, precuneus, inferior parietal lobule, posterior cingulate, occipital lobe, and temporal lobe. Increased and decreased DC values were clearly indicated through red and blue, respectively ($p < 0.01$, cluster > 40 voxels, AlphaSim corrected). Abbreviations: CU, corneal ulcer; NCs, normal controls; DC, degree centrality.
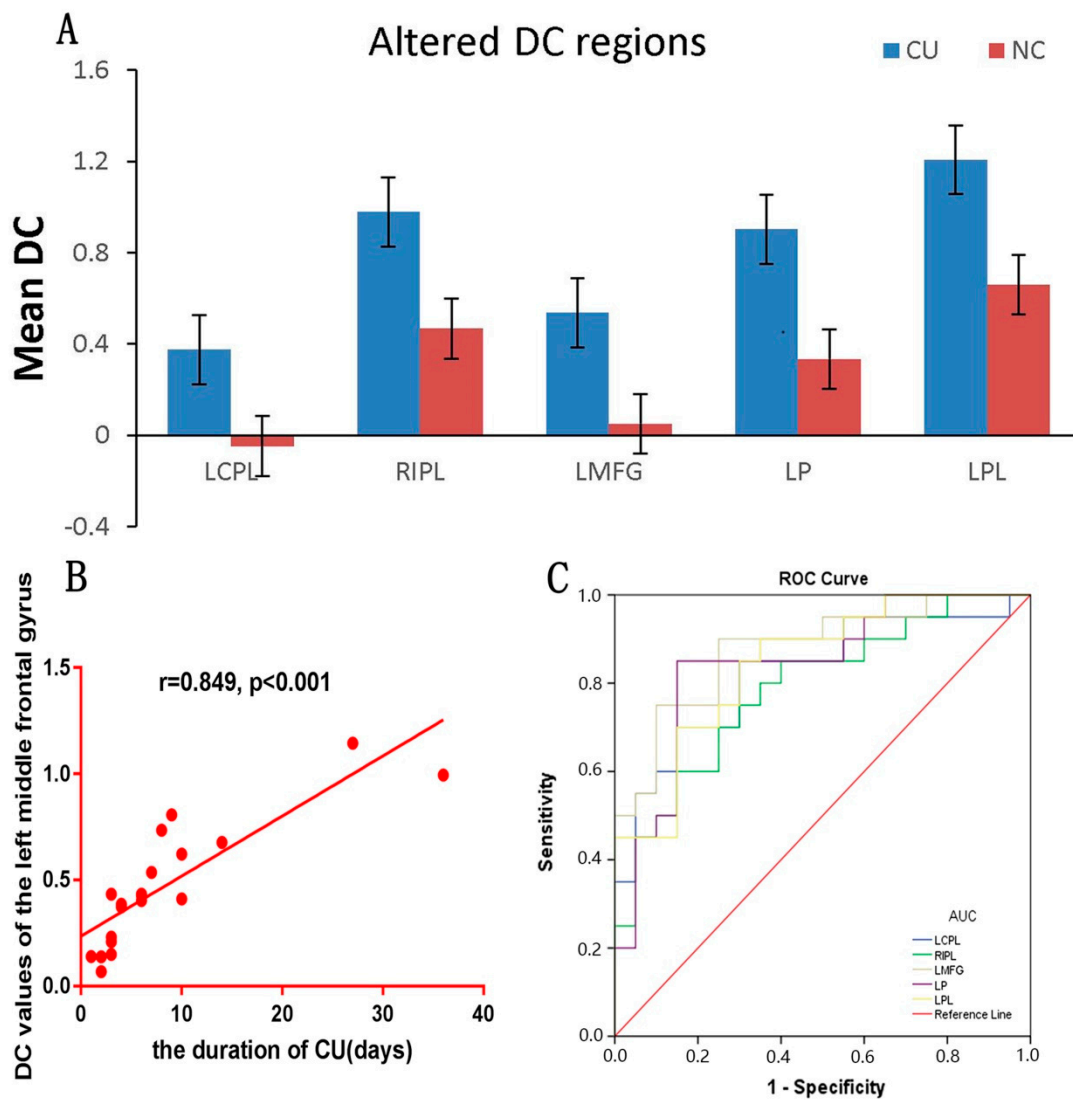
**Figure 5.** DC values of altered cerebrum regions (**A**) The average values of altered DC between two groups. (**B**) Correlations between the DC values of the left middle frontal gyrus and clinical performance. The DC values positively correlated with the duration of CU in the left middle frontal gyrus (r = 0.849, *p* < 0.001). (**C**) ROC curve analysis of the mean DC values for altered cerebrum regions. The AUCs were: LCPL, 0.822 (*p* < 0.001; 95% CI: 0.690–0.955); RIPL, 0.788 (*p* = 0.002; 95% CI: 0.647–0.928); LMFG, 0.878 (*p* < 0.001; 95% CI: 0.770–0.985); LP, 0.840 (*p* < 0.001; 95% CI: 0.713–0.967); and LPL, 0.842 (*p* < 0.001; 95% CI: 0.723–0.962). Abbreviations: DC, degree centrality; CU, corneal ulcer; NCs, normal controls; ROC, receiver operating characteristic; LCPL, left cerebellum posterior lobe; RIPL, right inferior parietal lobule; LPL, left parietal lobe, CI, confidence interval; LMFG, left middle frontal gyrus; LP, left precuneus.

## 4. Discussion

As far as we know, in patients with CU, the method we used in this study was the first to be utilized to figure out the synchronous neural activity changes. However, prior to this study, DC had been successfully used in many eye diseases (Figure 6) [15,16]. Patients with CU showed significant higher DC values in the left cerebellum posterior lobe, left middle frontal gyrus, left precuneus, left superior parietal lobule, and right inferior parietal lobule in our research. We confirmed that patients with CU and NCs could be distinguished via ROC curves.
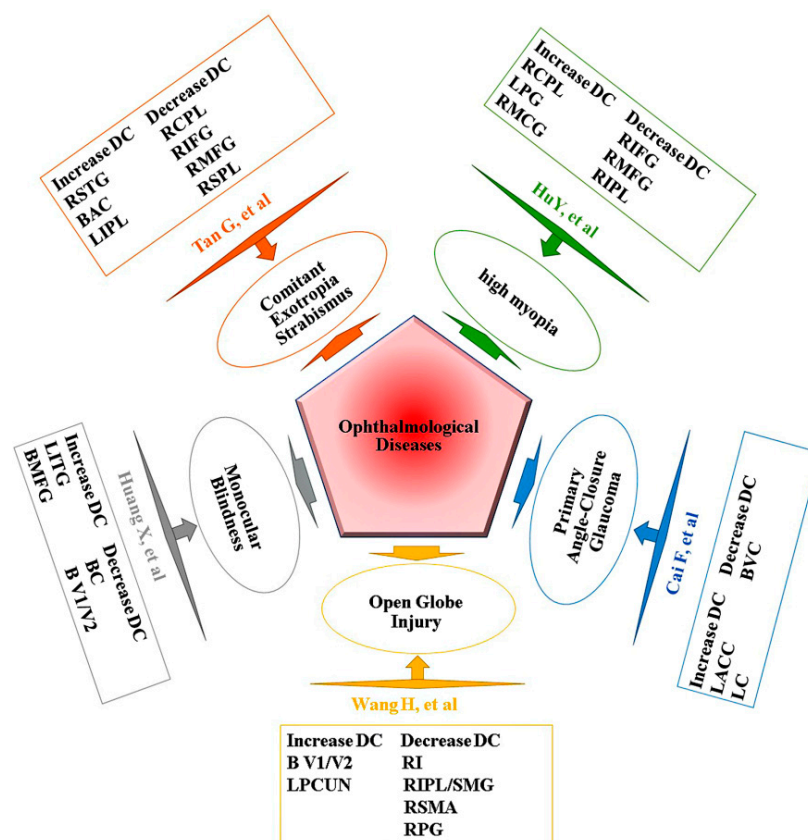
**Figure 6.** Previous studies using DC analysis. Abbreviations: DC, degree centrality; SMA, supplementary motor area; CPL, cerebellum posterior lobe; IFG, inferior frontal gyrus; SPL, superior parietal lobule; AC, anterior cingulate; IPL, inferior parietal lobule; PG, precentral gyrus; MCG, middle cingulate gyrus; LC, left caudate; VC, visual cortices; V1/V2, visual cortex I/II; MFG, middle frontal gyrus; PCUN, precuneus; RI, right insula; SMG, supramarginal gyrus; PG, postcentral gyrus; BC, bilateral cuneus; ACC, anterior cingulate cortex; STG, superior temporal gyrus; ITG, inferior temporal gyrus; L, left; R, right; B, bilateral.

Traditionally, relevant function of the cerebellum has been associated with movement coordination, and that the cerebellum posterior lobe controls the precise movement of eyeball is proven by some present studies [17]. Early studies in monkeys have shown that part of the cerebellum is related to the saccade and conjugates movements of the eyeball [18]. In addition, the cerebellum is connected to multiple visual areas [19], and eye movement and visual formation may have a close connection with the cerebellum posterior lobe. Patients with CU suffer from severe damage to the ocular surface, and eye movement can cause severe pain. Therefore, the activity of the cerebellum posterior lobe shows a significant increase in inhibiting eye movement. However, with the advancement and use of neuroimaging technology, we have deepened our understanding of the mechanisms of the brain, especially the cerebellum posterior lobe, regarding emotional processing [20]. Previous studies using positron emission tomography have found that patients with social anxiety have a greater possibility to show abnormal signals in the brain, manifesting as elevated cerebral blood flow. The investigators of these studies concluded that the cerebellum is related to anxiety [21]. The findings of this study are similar to those of previous studies. We performed fMRI scans on the patients prior to the operation, and the patients were generally nervous. Therefore, we believe that the high DC value was caused by the anxiety of patients and pain in the left cerebellum lobe.

Zhang found that the inferior parietal lobule, which is the kernel hub of the default mode network (DMN), exhibited a lower DC value in participants with higher negative coping scores [22]. The DMN is related to negative behavior, such as refusal to seek

assistance [23]. Obviously, our patients were actively seeking treatment and showed an increased DC value in the inferior parietal lobule. Similarly, a higher DC value was also shown in the precuneus (another key node of the DMN). In the medial parietal lobe, is where the anatomical position of the precuneus is located, and it has been associated with pain perception in humans [24]. Studies have shown that it works prominently in motor coordination and working memory [25,26]. We speculated that the pain caused by CU was responsible for the abnormal DC value observed in the left precuneus in the present research. An active network is located in the precuneus, taking part in maintaining the homeostasis of the central nervous system in the resting state [27]. The DMN consists of the medial temporal lobes, including the medial frontal cortex, inferior parietal cortex, posterior cingulate cortices, and anterior cingulate cortices. The brain regions with abnormal DC values in our experiment largely overlapped with the DMN. Thus, the possibility that CU causes DMN dysfunction cannot be ruled out.

From a different viewpoint, the inferior parietal lobule is involved spatial visual information processing related to the supramarginal gyrus, angular gyrus, and intraparietal sulcus [28]. Additionally, it is involved in various cognitive processes, such as visual-motion transformation [29], fine motion [30], and visual word recognition [31]. We concluded that CU caused corneal opacity, impairing the brain function from obtaining clear visual information. This resulted in dysfunction of the inferior parietal lobule, and the increased compensatory activity led to the recorded increase in DC value. Considering the involvement of the inferior parietal lobule in multiple cognitive processes, further research is warranted to demonstrate which of these processes lead to an increase in DC value.

The middle frontal gyrus is one of the well-studied gyri. It is part of the dorsal lateral prefrontal cortex, which is recognized by the medical community as being related to human cognitive and attention function [32]. At present, it is generally thought that cognitive impairment is a distinguishing feature of depression and pre-depression [33]. According to the Tear Film and Ocular Surface Society Dry Eye Workshop II, dry eye syndrome is often accompanied by depression [34]. Patients with CU suffer more than those with dry eye syndrome. Hence, it is reasonable to suggest that CU can cause depression in these patients, possibly explaining the observed increase in DC value in the middle frontal gyrus. (Figure 7) After further experimentation, we certainly proved that in the left middle frontal gyrus, the DC values was in proportion to the duration of CU to some extent. The findings indicate to some extents that the degree of depression in patients with CU is related to the course of disease. Collectively, the findings show that accessorial DC of the left prefrontal cortex is essential to maintain an appropriate level of cognitive and attention performance.
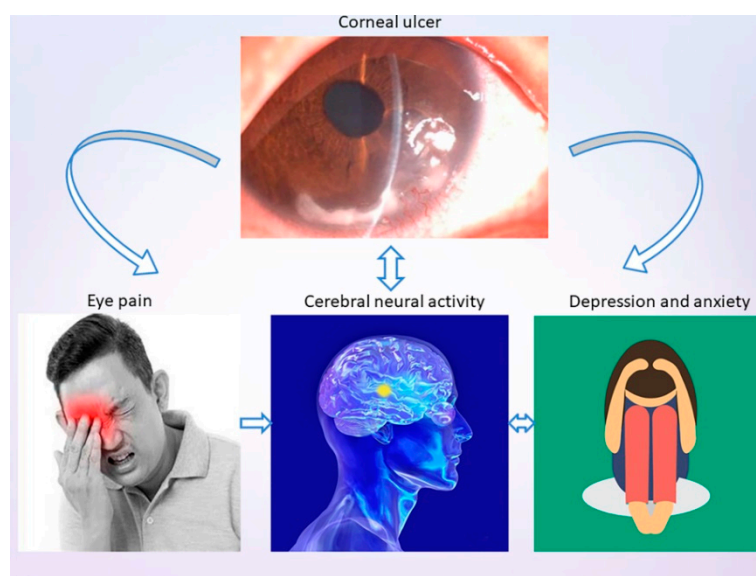


**Figure 7.** A schematic diagram of the relationship between corneal ulcer and eye pain and anxiety.

The superior parietal lobule, which is located near the occipital lobule and a part of the visual pathway [35], is associated with body position [36]. Anterior researches have demonstrated that the frontal lobe is responsible for the integration and coordination of visual-motor [37], while for the superior parietal lobule, its function is to transmit visual information to the frontal lobe [38]. Meanwhile, Segal et al. found that the functional connectivity between the left VI area and bilateral superior lobules was decreased for early blindness [39]. Our experiments have a clear finding that in the left superior parietal lobule, the DC value was increased in CU patients. We hypothesized that CU may impair visual-motor integration and coordination. From the conclusion of our discussion above, we have made such a summary table (Table 3) [40–44].

**Table 3.** Brain regions alternation and its potential impact.

| Brain Regions | Experimental Result | Brain Function | Anticipated Results |
|---|---|---|---|
| left cerebellum posterior lobe | CU > NC | sensorimotor, affective, and cognitive information [36] | Impairing both sensory and motor function; depression and anxiety [37] |
| right inferior parietal lobule | CU > NC | identify cognitive function, proprioception, and selective auditory attention [38] | Negative behavior and cognitive dysfunction. |
| left middle frontal gyrus | CU > NC | inhibition control, working memory, and emotional regulation [39] | Depression and anxiety |
| left precuneus | CU > NC | associated with pain perception and emotional control [40] | depression and anxiety |
| left superior parietal lobule | CU > NC | multiple cognitive processes and transmit visual information | impair the visual-motor integration and coordination |

Abbreviations: CU, corneal ulcer; NC, normal control.

The ROC curve analysis can be used to distinguish patients from NCs. In this analysis, the specificity and sensitivity of each encephalic region with changes in DC value were >70%. The results revealed that the AUCs of the left cerebellum posterior lobe, right inferior parietal lobule, left middle frontal gyrus, left precuneus, and left parietal lobe were 0.822, 0.788, 0.878, 0.840, and 0.842, respectively (all >0.7). This indicates that the DC value in these regions can serve as a reliable marker to distinguish patients with CU from NCs and is important for the exploration of neural mechanisms and the psychological state of patients with CU.

The experiment still has many limitations, such as the small sample size and lack of cover and the fact that the experimental limit is not very comprehensive (such as the influence of race). At the same time, further experimental investigation is also not enough (such as infectious and non-infectious ulcer brain activity variations). In future study, we will try to improve the deficiency of the experiment.

In conclusion, the results of this study proved that CU patients showed changes in synchronic neural activity in different cerebral regions, including visual-motor-related and pain-related brain regions. These alterations can be used for the exploration of neural mechanisms in patients with CU.

## References

1. Whitcher, J.P.; Srinivasan, M.; Upadhyay, M.P. Corneal blindness: A global perspective. *Bull. World Health Organ.* **2001**, *79*, 214–221. [PubMed]
2. Vyas, H.; Patel, M. Microbiological study in cases of corneal ulcer and clinical outcome. *Indian J. Clin. Exp. Ophthalmol.* **2017**, *3*, 454–457.
3. Lin, A.; Rhee, M.K.; Akpek, E.K.; Amescua, G.; Farid, M.; Garcia-Ferrer, F.J.; Varu, D.M.; Musch, D.C.; Dunn, S.P.; Mah, F.S. American Academy of Ophthalmology preferred practice pattern cornea and external disease panel. Bacterial keratitis preferred practice pattern®. *Ophthalmology* **2019**, *126*, P1. [CrossRef] [PubMed]
4. Bekiesińska-Figatowska, M.; Helwich, E.; Rutkowska, M.; Stankiewicz, J.; Terczyńska, I. Magnetic resonance imaging of neonates in the magnetic resonance compatible incubator. *Arch. Med. Sci.* **2016**, *12*, 1064–1070. [CrossRef]
5. Courrier, E.; Lepine, T.; Hor, G.; Fournier, C.; He, Z.; Chikh, M.; Urrea, C.; Al Anazi, F.-F.; Thuret, G.; Gain, P. Size of the lesions of superficial punctate keratitis in dry eye syndrome observed with a slit lamp. *Cornea* **2016**, *35*, 1004–1007. [CrossRef]
6. Borroni, D.; Rachwani-Anil, R.; González, J.M.S.; Rodríguez-Calvo-de-Mora, M.; de Lossada, C.R. Metagenome techniques to reduce diagnostic delay in Acanthamoeba keratitis. *Rom. J. Ophthalmol.* **2021**, *65*, 307–308. [CrossRef]
7. Gallon, P.; Parekh, M.; Ferrari, S.; Fasolo, A.; Ponzin, D.; Borroni, D. Metagenomics in ophthalmology: Hypothesis or real prospective? *Biotechnol. Rep.* **2019**, *23*, e00355. [CrossRef]
8. Borroni, D.; Romano, V.; Kaye, S.B.; Somerville, T.; Napoli, L.; Fasolo, A.; Gallon, P.; Ponzin, D.; Esposito, A.; Ferrari, S. Metagenomics in ophthalmology: Current findings and future prospectives. *BMJ Open Ophthalmol.* **2019**, *4*, e000248. [CrossRef]
9. Ouyang, J.; Yang, L.; Huang, X.; Zhong, Y.-L.; Hu, P.-H.; Zhang, Y.; Pei, C.-G.; Shao, Y. The atrophy of white and gray matter volume in patients with comitant strabismus: Evidence from a voxel-based morphometry study. *Mol. Med. Rep.* **2017**, *16*, 3276–3282. [CrossRef]
10. Shao, Y.; Huang, X.; Cai, F.-Q.; Hu, P.-H.; Zhong, Y.-L.; Zhang, Y.; Pei, C.-G.; Zhou, F.-Q.; Wei, R. Disturbed spontaneous brain-activity pattern in patients with optic neuritis using amplitude of low-frequency fluctuation: A functional magnetic resonance imaging study. *Neuropsychiatr. Dis. Treat.* **2015**, *11*, 3075–3083. [CrossRef]
11. Di Martino, A.; Zuo, X.N.; Kelly, C.; Grzadzinski, R.; Mennes, M.; Schvarcz, A.; Rodman, J.; Lord, C.; Castellanos, F.X.; Milham, M.P. Shared and distinct intrinsic functional network centrality in autism and attention-deficit/hyperactivity disorder. *Biol. Psychiatry* **2013**, *74*, 623–632. [CrossRef] [PubMed]
12. Garcia, I.G.; Jurado, M.Á.; Garolera, M.; Marqués-Iturria, I.; Horstmann, A.; Segura, B.; Pueyo, R.; Sender-Palacios, M.J.; Vernet-Vernet, M.; Villringer, A.; et al. Functional network centrality in obesity: A resting-state and task fMRI study. *Psychiatry Res. Neuroimaging* **2015**, *233*, 331–338. [CrossRef] [PubMed]
13. Lou, Y.; Huang, P.; Li, D.; Cen, Z.; Wang, B.; Gao, J.; Xuan, M.; Yu, H.; Zhang, M.; Luo, W. Altered brain network centrality in depressed Parkinson's disease patients. *Mov. Disord.* **2015**, *30*, 1777–1784. [CrossRef] [PubMed]
14. Yang, Y.-C.; Cai, G.-Q.; Yang, Q.-C.; Li, B.; Ge, Q.-M.; Li, Q.-Y.; Shi, W.-Q.; Min, Y.-L.; Liang, R.-B.; Shao, Y. Brain functional connectivity changes in patients with acute eye pain: A resting-state functional magnetic resonance imaging (fMRI) study. *Med. Sci. Monit.* **2021**, *27*, 930588. [CrossRef]
15. Cai, F.; Gao, L.; Gong, H.; Jiang, F.; Pei, C.; Zhang, X.; Zeng, X.; Huang, R. Network centrality of resting-state fMRI in primary angle-closure glaucoma before and after surgery. *PLoS ONE* **2015**, *10*, e0141389. [CrossRef]
16. Hu, Y.X.; He, J.R.; Yang, B.; Huang, X.; Li, Y.P.; Zhou, F.Q.; Xu, X.X.; Zhong, Y.L.; Wang, J.; Wu, X.R. Abnormal resting-state functional network centrality in patients with high myopia: Evidence from a voxel-wise degree centrality analysis. *Int. J. Ophthalmol.* **2018**, *11*, 1814–1820.
17. Herzfeld, D.J.; Kojima, Y.; Soetedjo, R.; Shadmehr, R. Encoding of action by the Purkinje cells of the cerebellum. *Nature* **2015**, *526*, 439–442. [CrossRef]
18. Joshi, A.C.; Das, V.E. Muscimol inactivation of caudal fastigial nucleus and posterior interposed nucleus in monkeys with stra-bismus. *J. Neurophysiol.* **2013**, *110*, 1882–1891. [CrossRef]
19. Strick, P.L.; Dum, R.P.; Fiez, J.A. Cerebellum and nonmotor function. *Annu. Rev. Neurosci.* **2009**, *32*, 413–434. [CrossRef]
20. Adamaszek, M.; D'Agata, F.; Ferrucci, R.; Habas, C.; Keulen, S.; Kirkby, K.C.; Leggio, M.; Mariën, P.; Molinari, M.; Moulton, E.; et al. Consensus paper: Cerebellum and emotion. *Cerebellum* **2017**, *16*, 552–576. [CrossRef]

21. Liu, W.; Liu, H.; Wei, D.; Sun, J.; Yang, J.; Meng, J.; Wang, L.; Qiu, J. Abnormal degree centrality of functional hubs associated with negative coping in older Chinese adults who lost their only child. *Biol. Psychol.* **2015**, *112*, 46–55. [CrossRef]

22. Zhang, S.; Li, C.S.R. Functional clustering of the human inferior parietal lobule by whole-brain connectivity mapping of rest-ing-state functional magnetic resonance imaging signals. *Brain Connect.* **2014**, *4*, 53–69.

23. Zhu, X.; Wang, X.; Xiao, J.; Liao, J.; Zhong, M.; Wang, W.; Yao, S. Evidence of a dissociation pattern in resting-state default mode network connectivity in first-episode, treatment-naive major depression patients. *Biol. Psychiatry* **2012**, *71*, 611–617. [CrossRef]

24. Goffaux, P.; Girard-Tremblay, L.; Marchand, S.; Daigle, K.; Whittingstall, K. Individual differences in pain sensitivity vary as a function of precuneus reactivity. *Brain Topogr.* **2014**, *27*, 366–374. [CrossRef]

25. Wallentin, M.; Weed, E.; Østergaard, L.; Mouridsen, K.; Roepstorff, A. Accessing the mental space—Spatial working memory processes for language and vision overlap in precuneus. *Hum. Brain Mapp.* **2008**, *29*, 524–532. [CrossRef]

26. Wenderoth, N.; Debaere, F.; Sunaert, S.; Swinnen, S.P. The role of anterior cingulate cortex and precuneus in the coordination of motor behaviour. *Eur. J. Neurosci.* **2005**, *22*, 235–246. [CrossRef]

27. Raichle, M.E.; MacLeod, A.M.; Snyder, A.Z.; Powers, W.J.; Gusnard, D.A.; Shulman, G.L. A default mode of brain function. *Proc. Natl. Acad. Sci. USA* **2001**, *98*, 676–682. [CrossRef]

28. Egner, T.; Monti, J.M.P.; Trittschuh, E.H.; Wieneke, C.A.; Hirsch, J.; Mesulam, M.-M. Neural integration of top-down spatial and feature-based information in visual search. *J. Neurosci.* **2008**, *28*, 6141–6151. [CrossRef]

29. Moretti, D.V. Increase of EEG Alpha3/Alpha2 power ratio detects inferior parietal lobule atrophy in mild cognitive im-pairment. *Curr. Alzheimer Res.* **2018**, *15*, 443–451. [CrossRef]

30. Reed, T.; Pierce, W.M., Jr.; Turner, D.M.; Markesbery, W.R.; Butterfield, D.A. Proteomic identification of nitrated brain proteins in early Alzheimer's disease inferior parietal lobule. *J. Cell. Mol. Med.* **2009**, *13*, 2019–2029. [CrossRef]

31. Sliwinska, M.W.; James, A.; Devlin, J.T. Inferior parietal lobule contributions to visual word recognition. *J. Cogn. Neurosci.* **2015**, *27*, 593–604. [CrossRef]

32. Song, P.; Lin, H.; Liu, C.; Jiang, Y.; Lin, Y.; Xue, Q.; Xu, P.; Wang, Y. Transcranial magnetic stimulation to the middle frontal gyrus during attention modes induced dynamic module reconfiguration in brain networks. *Front. Neuroinform.* **2019**, *13*, 22. [CrossRef]

33. Groenewold, N.A.; Opmeer, E.M.; de Jonge, P.; Aleman, A.; Costafreda, S.G. Emotional valence modulates brain functional abnormalities in depression: Evidence from a meta-analysis of fMRI studies. *Neurosci. Biobehav. Rev.* **2013**, *37*, 152–163. [CrossRef]

34. Han, S.B.; Yang, H.K.; Hyon, J.Y.; Wee, W.R. Association of dry eye disease with psychiatric or neurological disorders in elderly patients. *Clin. Interv. Aging* **2017**, *12*, 785–792. [CrossRef]

35. Ioannides, A.A.; Liu, L.; Poghosyan, V.; Saridis, G.A.; Gjedde, A.; Ptito, M.; Kupers, R. MEG reveals a fast pathway from somatosensory cortex to occipital areas via posterior parietal cortex in a blind subject. *Front. Hum. Neurosci.* **2013**, *7*, 429. [CrossRef]

36. Felician, O.; Romaiguère, P.; Anton, J.-L.; Nazarian, B.; Roth, M.; Poncet, M.; Roll, J.-P. The role of human left superior parietal lobule in body part localization. *Ann. Neurol.* **2004**, *55*, 749–751. [CrossRef]

37. Iacoboni, M.; Zaidel, E. Interhemispheric visuo-motor integration in humans: The role of the superior parietal cortex. *Neuropsychologia* **2004**, *42*, 419–425. [CrossRef]

38. Caminiti, R.; Ferraina, S.; Johnson, P.B. The sources of visual information to the primate frontal lobe: A novel role for the superior parietal lobule. *Cereb. Cortex* **1996**, *6*, 319–328. [CrossRef]

39. Segal, E.; Petrides, M. The anterior superior parietal lobule and its interactions with language and motor areas during writing. *Eur. J. Neurosci.* **2012**, *35*, 309–322. [CrossRef]

40. Yang, H.; Wang, N.; Luo, X.; Lv, H.; Liu, H.; Li, Y.; Fan, G. Cerebellar atrophy and its contribution to motor and cognitive performance in multiple system atrophy. *NeuroImage Clin.* **2019**, *23*, 101891. [CrossRef]

41. Jia, Z.; Peng, W.; Chen, Z.; Sun, H.; Zhang, H.; Kuang, W.; Huang, X.; Lui, S.; Gong, Q. Magnetization transfer imaging of treatment-resistant depression. *Radiology* **2017**, *284*, 521–529. [CrossRef]

42. Morita, T.; Saito, D.N.; Ban, M.; Shimada, K.; Okamoto, Y.; Kosaka, H.; Okazawa, H.; Asada, M.; Naito, E. Self-face recognition begins to share active region in right inferior parietal lobule with proprioceptive illusion during adolescence. *Cereb. Cortex* **2018**, *28*, 1532–1548. [CrossRef]

43. Wang, Y.; Zhu, W.; Xiao, M.; Zhang, Q.; Zhao, Y.; Zhang, H.; Chen, X.; Zheng, Y.; Xia, L.-X. Hostile attribution bias mediates the relationship between structural variations in the left middle frontal gyrus and trait angry rumination. *Front. Psychol.* **2018**, *9*, 526. [CrossRef]

44. Yuan, C.; Zhu, H.; Ren, Z.; Yuan, M.; Gao, M.; Zhang, Y.; Li, Y.; Meng, Y.; Gong, Q.; Lui, S.; et al. Precuneus-related regional and network functional deficits in social anxiety disorder: A resting-state functional MRI study. *Compr. Psychiatry* **2018**, *82*, 22–29. [CrossRef]